

DOPPLER SHIFTED CYCLOTRON RESONANCE IN CADMIUM

O. V. KONSTANTINOV, V. G. SKOBOV, V. V. LAVROVA, L. M. FISHER, and V. A. YUDIN

A. F. Ioffe Physico-technical Institute, USSR Academy of Sciences; All-union Electrotechnical Institute

Submitted February 7, 1972

Zh. Eksp. Teor. Fiz. 63, 224-241 (July, 1972)

The Doppler-shifted cyclotron resonance in cadmium in a magnetic field $H \parallel [0001]$ is studied theoretically and experimentally in the radio-frequency region. The resonance is due to carriers with extreme displacements during the cyclotron period. Dispersion of the dielectric constant due to the resonance leads to the appearance of weakly damped waves-dopplerons. It is found that beside dopplerons due to lens electrons, there exist hole dopplerons related to orbits near the central cross section of the monster. Excitation of this type of doppleron in cadmium plates leads to surface-resistance oscillations of the electron doppleron. The regions of existence of both types of doppleron are bounded from the weak magnetic field side. The effect of the shape of the Fermi surface on the doppleron spectrum and position of the boundary fields is studied. The shape of the electron lens is determined by comparing the theoretical and experimental results. The value of the derivative of the monster cross section area with respect to momentum derived from oscillation period measurements is in agreement with the monster model employed.

1. INTRODUCTION

WE have previously^[1] investigated theoretically and experimentally the weakly-damped electromagnetic waves (dopplerons) that propagate in cadmium in a magnetic field parallel to the hexagonal axis. The possibility of propagation of these waves is connected with the Doppler-shifted cyclotron resonance (DSCR) of the electrons of the lens section of the Fermi surface in the third Brillouin zone. When the DSCR condition $q \equiv u_0\kappa/2\pi = 1$ is satisfied (κ is the wave vector and u_0 is the displacement of the electrons at the limiting point of the lens along the magnetic field during the cyclotron period), the transverse nonlocal conductivity of the lens electrons has a singularity. Near the singularity, the conductivity of the electrons is much higher than its local limit, and consequently is not compensated for by the conductivity of the holes. In the local limit, the hole conductivity of the metal is close to zero, since the electron and hole densities in cadmium are equal. With decreasing wavelength, the conductivity increases and has a singularity at $q \rightarrow 1$, and this makes the doppleron propagation possible. Wave excitation in a plate leads to oscillations of the surface impedance as a function of the magnetic field. The period of the oscillations corresponds to a unity change in the number of wavelengths subtended by the thickness of the plate. The dopplerons observed in^[1] exist in a limited field interval, and their distinguishing feature is the significant change in the period of the oscillations with changing magnetic field. The period increases monotonically with increasing magnetic field H , owing to the dependence of the wave vector on H . The field interval in which the doppleron is observed is restricted by the clearly defined lower limiting field, and a smooth decrease of the oscillation amplitude takes place on the strong-field side. The limiting field is proportional to the cube root of the frequency, and its value is determined by the shape of the Fermi surface. In strong fields, the period of the oscillations

in the region where their amplitude decreases changes little with the magnetic field, and approaches the period of the radio-frequency size effect of Gantmakher and Kaner.

The nonlocal conductivity can have resonant singularities connected not only with the electrons of the limiting point, but also with carriers on other sections of the Fermi surface. The Doppler-shifted cyclotron resonance leads to singularities of the conductivity for any group of carriers that has an extremal displacement in the cyclotron period^[2-4]. We have investigated the propagation of a doppleron due to Doppler-shifted resonance of the electrons and the holes in cadmium in a magnetic field parallel to the hexagonal axis. The displacement of the holes is maximal in the immediate vicinity of the maximal cross section of the monster, and this group of carriers also gives rise to a singularity of the nonlocal conductivity, just as the lens electrons.

2. MEASUREMENT PROCEDURE

We investigated the dependence of the derivative of the surface resistance $\partial R/\partial H$ of single-crystal cadmium plates as a function of the magnetic field. The field was normal to the surface of the sample. The measurements were made at frequencies in the interval from 0.6 to 3 MHz. The measurement procedure is described in detail in^[1,5].

12×25 mm samples, 0.38, 0.57, and 0.91 mm thick were cut by the electric-spark method from a single crystal in such a way that the normal to the plate coincided with the direction of the hexagonal axis, and the large axis of the sample was parallel to the $[11\bar{2}0]$ axis. The sample was oriented by x-ray diffraction¹⁾. The resistance ratio was $\rho(300^\circ\text{K})/\rho(4.2^\circ\text{K}) = 3 \times 10^4$.

A magnetic field up to 16 kOe was produced with the aid of an electromagnet which was fed from a motor-

¹⁾The authors thank A. P. Naumkin for the x-ray diffraction measurements.

generator. The field was electronically stabilized accurate to 0.05%. The constant magnetic field was modulated at a low frequency (10 Hz) and an amplitude up to 150 Oe with the aid of additional coils. The coils were fed from a low-frequency generator and a power amplifier.

To perform the measurements, the sample was placed in a flat measuring coil and was secured in a polystyrene holder in such a way that the axes [0001] and [10 $\bar{1}$ 0] were in the horizontal plane. The magnetic field direction relative to the crystallographic axes could be varied by rotating the magnet in the horizontal plane through 360° and in two vertical planes through $\pm 5^\circ$, with accuracy $\pm 15'$. The orientation at which H was parallel to [0001] was determined from the symmetry of the plots of $\partial R/\partial H$ against the angle θ between the direction of the magnetic field and the [0001] axis, and also from the angular dependence of the doppleron amplitude. All the measurements were performed at temperatures from 1.6 to 4.2°K. A signal proportional to $\partial R/\partial H$ was fed to the Y coordinate of an automatic potentiometer; a voltage proportional to the magnetic field was fed to the X coordinate from a Hall pickup. We used a specially developed automatic-plotting potentiometer with sensitivity up to 3.3 $\mu\text{V}/\text{cm}$ and with an approximate recording error 0.5%^[6]. Each $\partial R/\partial H$ plot against the magnetic field was calibrated directly during the measurements with the aid of an NMR magnetometer with running water, a modified variant of the instrument described in^[7]. The total X-coordinate measurement error did not exceed 1%.

3. MEASUREMENT RESULTS

Impedance oscillations connected with the excitation of the doppleron by the lens electrons (electronic doppleron) were observed for all the investigated samples, in agreement with the results of^[1]. The oscillation amplitude was 3–5 times larger than before, owing to the better quality of the crystals (resistance ratio $\rho(300^\circ\text{K})/\rho(4.2^\circ\text{K}) = 3 \times 10^4$ as against 1×10^4 of the previously employed crystals). The range of the oscillations of the electronic doppleron extended to lower fields than observed in^[1]. Thus, at a frequency $f = 1$ MHz, the lower limit of the electronic doppleron H_{min}^e turned out to be 6.2 kOe as against the 7.5 kOe obtained in^[1]. This is apparently also due to the better quality of the crystals. In magnetic fields weaker than H_{min}^e we observed surface-impedance oscillations with small periods. Although the amplitude of these oscillations was approximately 1/50th the maximum amplitude of the electronic doppleron oscillations, they could be resolved by using higher gain.

A typical plot of $\partial R/\partial H$ against the field is shown in Fig. 1. The large-amplitude oscillations at $H > 7.5$ kOe are connected with a propagation of the electronic doppleron, and at $H < 7.5$ kOe one can see weak oscillations with a smaller period. The amplitude of the latter increased with decreasing temperature, and the measurements were therefore performed mainly at $T = 1.6^\circ\text{K}$.

A typical plot of $\partial R/\partial H$ at a higher gain is shown in Fig. 2. We see that these oscillations are distinguished by the presence of a lower limit $H_{\text{min}}^h = 5.9$ kOe (for

$f = 1.91$ MHz). In fields stronger than 7.5 kOe, the signal due to the electronic doppleron increased sharply, and the short-period oscillations could not be seen against its background. At $f = 1$ MHz, the short-period oscillations are observed in the field interval from 4.7 to 6.2 kOe. With increasing frequency, the limits of the interval shift towards stronger fields in proportion to $f^{1/3}$. When the field is increased from H_{min}^h to H_{min}^e , the amplitude of the oscillations increases, reaches a maximum, and then decreases.

When the magnetic field is inclined to the [0001] axis, the amplitude of the oscillations decreases and the interval of magnetic fields in which the oscillations were observed increases. The broadening of the region of the short-period oscillations is due to the sharp decrease of the amplitude of the electronic doppleron with increasing angle and to the ensuing shifts of the observed boundary H_{min}^e towards stronger fields. The maximum angle at which the short-period oscillations can still be seen is 12.5° .

The observed oscillations are approximately periodic in the direct magnetic field, although the period increases by 20–30% when the field changes from H_{min}^h to H_{min}^e . Figure 3 shows the dependence of the period of the oscillations on the magnetic field for three samples of different thickness. As seen from the plots, the field dependence of the period ΔH has the form of a curve with saturation, and the limiting values of the period are determined only by the sample thickness d ($\Delta H \propto 1/d$).

Thus, the characteristic features of the observed oscillations are: 1) the limited region of the fields in which they are observed, 2) the shift of this region towards stronger fields with increasing frequency f , in proportion to $f^{1/3}$, and 3) the increase of the period of the oscillations with increasing field. Similar regularities hold for the oscillations due to the excitation of the electronic doppleron. This analogy suggests that the short-period oscillations are connected with the doppler-shifted cyclotron resonance of other carriers (holes). By starting from this assumption, we can obtain the maximum displacement of the holes during the cyclotron period. The displacement is proportional to

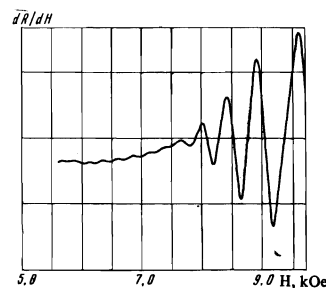


FIG. 1

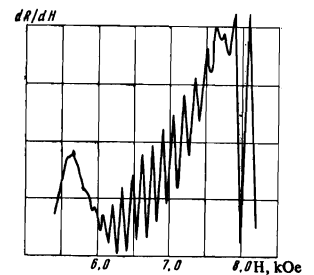


FIG. 2

FIG. 1. Dependence of the derivative of the surface resistance of a single-crystal cadmium plate on the constant magnetic field H . The normal to the surface of the plate and the vector H are parallel to the hexagonal axis; the plate thickness is $d = 0.57$ mm, the frequency of the alternating field is $f = 1.74$ MHz.

FIG. 2. Short-period oscillations of the derivative $\partial R/\partial H$, obtained for a sample $d = 0.91$ mm thick at a frequency $f = 1.91$ MHz.

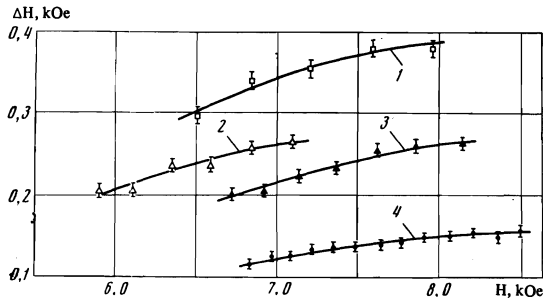


FIG. 3. Dependence of the period of the oscillations on the magnetic field for different samples and different frequencies: 1) $d = 0.38$ mm, $f = 2.1$ MHz; 2) $d = 0.57$ mm, $f = 1.75$ MHz; 3) $d = 0.57$ mm, $f = 2.54$ MHz; 4) $d = 0.91$ mm, $f = 2.74$ MHz. The period was determined from the maxima of the oscillations of $\partial R/\partial H$, the position of the point along the abscissa axis corresponds to the right-hand extremum of the pair from which the period was determined.

the derivative $\partial S^h/\partial k_z$, where S^h is the area of the hole orbit in wave-vector space, k_z is the longitudinal component of the wave vector, and $z \parallel H$. The limiting value of the doppleron oscillation period $(\Delta H)_{\max}$, which coincides with the period of the Gantmakher-Kaner size effect^[8], makes it possible to determine the maximum value of the derivative:

$$\left(\frac{\partial S^h}{\partial k_z}\right)_{\max} = \frac{eHd}{2\pi\hbar c} \Delta H_{\max}, \quad (1)$$

where e is the absolute value of the electron charge and c is the speed of light. The derivative calculated from this formula turned out to be

$$(\partial S^h/\partial k_z)_{\max} = 2.2 \pm 0.1 \text{ \AA}^{-1}. \quad (2)$$

for all the investigated samples. We shall show below that the short-period oscillations are connected with the DSCR of the holes of the monster. To this end, we examine first the Fermi surface of cadmium.

4. THE FERMI SURFACE OF CADMIUM

The Fermi surface of cadmium was investigated by various methods^[9-17]. Grassie^[9] used the de Haas-van Alphen effect to measure the areas of the external sections of the Fermi surface at the different magnetic-field orientations. The radio-frequency size effect was used to measure its geometrical dimensions^[15-17]. Stark and Falicov^[18] calculated theoretically the shape of the Fermi surface on the basis of a model pseudo-potential. According to the results of these calculations, it consists of three parts: a small hole "pyramid" in the first energy zone, a hole "monster" in the second zone, and an electron "lens" in the third zone. The forms of these surfaces and their positions in the Brillouin zone are shown in Fig. 4. Figure 5 shows a three-dimensional picture of the monster drawn in the expanded zone scheme to demonstrate more clearly the intersection of the monster by planes perpendicular to the hexagonal axis. It should be borne in mind that the Brillouin zone contains two figures, each of which is made up of three pieces located at the corners of a six-face prism. Figure 6 shows plots of $\partial S/\partial k_z$ against k_z for the lens, monster, and pyramid. These plots were calculated on the basis of the graphic data of Jones, Goodrich, and Falicov^[17]. The accuracy of such a construction is of the order of 10%. It is seen

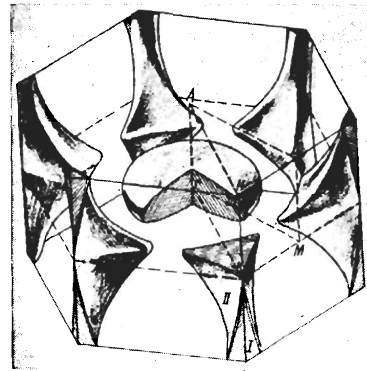


FIG. 4. Model of Fermi surface of cadmium in the almost-free electron approximation^[17,18]: I—hole pyramid in the first Brillouin zone, II—hole monster in the second zone, III—electron lens in the third zone.

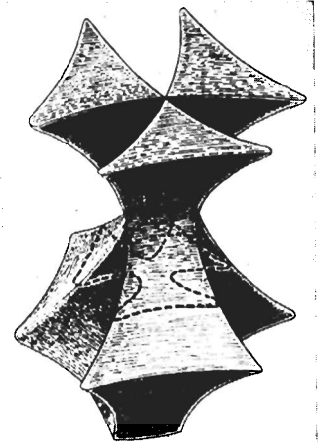


FIG. 5. Hole monster in the expanding-zone scheme. The axis of the figure coincides with the edge KH zone of the Brillouin zone. The upper surface is the section of the monster in the Γ KM plane. The dashed line shows the section in the AHL plane (convex triangle), and also two intermediate cross-sections.

from Fig. 6 that at $H \parallel [0001]$ there are in cadmium three maximal values of $\partial S/\partial k_z$: $(\partial S^p/\partial k_z)_{\max} = 9.4 \text{ \AA}^{-1}$ at the limiting point of the lens ($k_z = 0.28 \text{ \AA}^{-1}$), $(\partial S^h/\partial k_z)_{\max} = 2.5 \text{ \AA}^{-1}$ near the maximum cross section of the monster, and $(\partial S^l/\partial k_z)_{\max} = 0.25 \text{ \AA}^{-1}$ at the pyramid. Thus, the maximum value of the derivative for the monster is close to the one given in (2), which characterizes the short-period oscillations of the impedance. This means that the latter are connected with the Doppler-shifted cyclotron resonance of the holes of the monster.

5. THEORY

The qualitative picture of the propagation of electromagnetic wave near the Doppler-shifted cyclotron resonance of the holes of the monster is fully analogous in general outline to the picture used by us to describe the electronic doppleron. In both cases, the wave propagation is possible because of the sharp increase of the non-dissipative part of the conductivity as the doppleron wavelength approaches the maximum displacement of the carriers during the cyclotron period. The wavelength remains somewhat larger than the maximum displacement. The latter circumstance means that the electronic doppleron does not experience collisionless cyclotron absorption at all, and the hole doppleron is not subject to collisionless absorption by holes. The point is that the wavelength of this

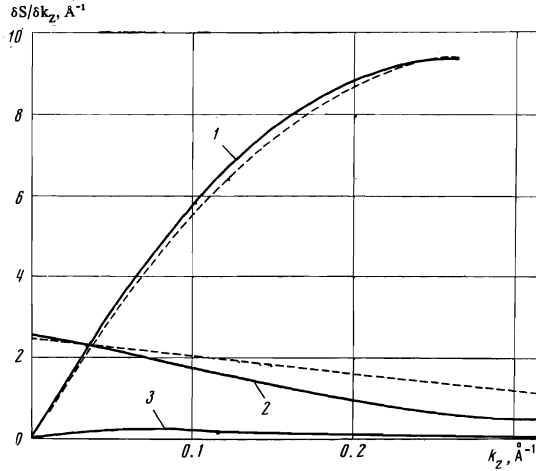


FIG. 6. Plots of $\partial S/\partial k_z$: 1—for lens, 2—for monster, 3—for pyramid. The solid curves were obtained on the basis of the graphic data of [17], and the dashed curves correspond to the models employed by us for the lens ($n = 2$) and monster. k_z is reckoned from the Γ KM plane of the Brillouin zone for curves 1 and 2, and from the AHL plane for curve 3.

dippleron is approximately one-quarter the displacement of the electrons at the limiting point of the lens. If the edges of the lens are smoothly rounded off, there are always on the lens electrons whose displacement is one-quarter the displacement at the limiting point, and the conditions of the Doppler-shifted cyclotron resonance are satisfied for these electrons. As the result, these electrons cause collisionless damping of the hole doppleron. The value of the collisionless absorption depends on the shape of the lens. It is quite natural to expect the dispersion of the non-dissipative part of the electronic conductivity also to be dependent on this shape. To study the properties of the wave it is therefore necessary to calculate the nonlocal conductivities of the electrons and holes in such a way that variation of the shape of the Fermi surface is possible.

1. Nonlocal conductivity of the anisotropic metal. A general expression for the nonlocal conductivity is given in the review [19] (see p. 626) in the case of closed carrier orbits. This expression can be transformed into

$$\sigma_{\alpha\beta}(\kappa, \omega) = \frac{e^2}{2\pi^2 \hbar^3} \int \frac{dp_z}{|m(p_z)|} \sum_{M=-\infty}^{\infty} \frac{P_M^\alpha (P_M^\beta)^*}{\nu + i(M\Omega + \kappa \langle v_z \rangle - \omega)}, \quad (3)$$

$$P_M^\alpha = \frac{m(p_z)}{2\pi} \int_0^{2\pi} d\varphi v_\alpha(\varphi) \exp\left\{iM\left(\varphi - \frac{\pi}{2}\right)\right\} \times \exp\left\{-\frac{i}{\Omega} \int_{\pi/2}^{\varphi} d\varphi' \kappa [v(\varphi') - \langle v \rangle]\right\}. \quad (4)$$

Here ω and κ are the frequency and the wave vector of the electromagnetic wave, p_z is the projection of the electron momentum on the magnetic field, which in turn is directed along the z axis, $m(p_z)$ is the cyclotron mass, ν is the collision frequency, and $\Omega(p_z) = e\hbar/mc$ is the cyclotron frequency. $v_\alpha(\varphi)$ is the component of the electron velocity on the Fermi surface, and $\langle v_\alpha \rangle$ is the mean value of the velocity during the cyclotron period. Obviously, the vector $\langle v \rangle$ is directed along the magnetic field.

The general expression (3) can be greatly simplified if the wave vector κ and the magnetic field H are directed along one of the principal crystallographic axes. We shall henceforth confine ourselves only to this case. The simplification is due to the possibility of integrating in (4) with respect to the variable φ . The electron lens has rotational symmetry, and the variable φ has the meaning of the azimuthal angle, while the transverse projections v_α are proportional to the sine and the cosine of this angle. The longitudinal velocity is independent of the angle. Therefore the integral in (4) can be evaluated in elementary fashion. For a hole monster having a threefold symmetry, this calculation is more complicated. The variable φ no longer has so simple a geometrical meaning. It is connected with the individual time of revolution τ of the electron on the closed orbit in the plane $p_z = \text{const}$ by the relation

$$\varphi = \Omega(p_z) \tau, \quad \tau = \int \frac{dp_l}{mv_\perp}, \quad (5)$$

where dp_l is the element of the arc of the orbit and v_\perp is the projection of the velocity on the plane of the orbit. It should be noted, however, that at symmetrical points of the orbit the values of the variable φ coincide as before with the azimuthal angles of these points. Thus, for example, if the orbit has the form of an equilateral triangle, then the values of the variable φ for its vertices (or for the midpoint of the sides, depending on the choice of the origin) are 0, $2\pi/3$, and $4\pi/3$. Using this circumstance, we can represent the velocity components in the form of the following Fourier series:

$$v_x(\varphi) = v_0 \left[\cos \varphi + \sum_{l=1}^{\infty} \xi_l \cos(1-s)l\varphi + \sum_{l=1}^{\infty} \eta_l \cos(1+s)l\varphi \right], \quad (6a)$$

$$v_y(\varphi) = v_0 \left[\sin \varphi + \sum_{l=1}^{\infty} \xi_l \sin(1-s)l\varphi + \sum_{l=1}^{\infty} \eta_l \sin(1+s)l\varphi \right], \quad (6b)$$

$$v_z(\varphi) = \langle v_z \rangle \left[1 + \sum_{l=1}^{\infty} \xi_l \sin sl\varphi \right]. \quad (6c)$$

Here s is the order of the symmetry ($s = 3$ for the monster). If one of the symmetrical directions is chosen as the reference for φ , then

$$v_x(0) = v_0 \left[1 + \sum_{l=1}^{\infty} (\xi_l + \eta_l) \right], \quad v_y(0) = 0; \quad (7)$$

It is easy to verify that for $\varphi = 2\pi/s$

$$v_x(2\pi/s) = v_x(0) \cos(2\pi/s), \quad v_y(2\pi/s) = v_x(0) \sin(2\pi/s). \quad (8)$$

The expansions (6a) and (6b) were obtained on the basis of these properties.

The quantities ξ_l , η_l , and ζ_l , which characterize the corrugation, are in general functions of p_z . The meaning of the quantity v_0 can be established by calculating the area of the orbit in k -space:

$$S = \frac{1}{\hbar^2} \int_0^{2\pi} p_x \frac{dp_y}{d\varphi} d\varphi. \quad (9)$$

The integral (9) can be calculated by using the equations of motion

$$mv_x = dp_y / d\varphi, \quad mv_y = -dp_x / d\varphi \quad (10)$$

and expressions (6a) and (6b). The calculation yields

$$S = \pi \left(\frac{v_0 m}{\hbar} \right)^2 \left[1 + \sum_{l=1}^{\infty} \frac{\xi_l^2}{1-sl} + \sum_{l=1}^{\infty} \frac{\eta_l^2}{1+sl} \right]. \quad (11)$$

This relation connects the parameter v_0 with the area of the orbit and with the corrugation parameters. The pulsations of the longitudinal velocity, which are described by (6c), lead in the general case to a rather complicated dependence of the conductivity on the wave vector κ . It is determined by the exponential factor in (4)

$$\begin{aligned} & \exp \left\{ -i \frac{1}{\Omega_h} \int_{\pi/2}^{\pi} d\varphi' \kappa [v(\varphi') - \langle v \rangle] \right\} \\ & = \exp \left\{ -i \frac{\kappa u_h}{2\pi} \sum_{l=1}^{\infty} \frac{\xi_l}{ls} \left[\cos \frac{ls\pi}{2} - \cos ls\varphi \right] \right\}, \end{aligned} \quad (12)$$

where $u_h = 2\pi \langle v_z \rangle / \Omega_h$ is the average displacement of the holes during the cyclotron period.

We are interested here principally in the case

$$\kappa u_h / 2\pi \ll 1, \quad (13)$$

when the wavelength exceeds the average displacement during the period. One should expect the argument of the exponential (12) to be small in this case, since it contains the small factor $1/ls$. The exponential (12) can be expanded in a series, retaining only terms of order $\kappa u_h / 2\pi$. Calculation shows that these terms give rise to terms of the type $(\kappa u_h \xi_l / 4\pi ls)^2$ in the conductivity. In comparison with the terms ξ_l^2 and η_l^2 , they contain the small factor $(\kappa u_h / 4\pi ls)^2$. We can therefore neglect the pulsations of the longitudinal velocity in comparison with the pulsations of v_x and v_y .

Let us calculate the nonlocal conductivity for a circularly polarized electric field.

$$\sigma^{\pm} = \sigma_{xx} \pm i\sigma_{yx}. \quad (14)$$

The conductivities σ^+ and σ^- pertain to the cases when the electric vector of the wave rotates in the direction of the cyclotron rotation of the holes and electrons, respectively. The expression for the conductivity σ^{\pm} takes the form

$$\begin{aligned} \sigma^{\pm} = & \frac{e^2}{4\pi^2 \hbar^3} \sum \int \frac{dp_z}{|m|} (mv_0)^2 \left\{ \frac{1}{v + i(\pm \Omega + \kappa \langle v_z \rangle - \omega)} \right. \\ & + \sum_{l=1}^{\infty} \left[\frac{\xi_l^2}{v + i(\mp(1-ls)\Omega + \kappa \langle v_z \rangle - \omega)} \right. \\ & \left. \left. + \frac{\eta_l^2}{v + i(\mp(1+ls)\Omega + \kappa \langle v_z \rangle - \omega)} \right] \right\}, \end{aligned} \quad (15)$$

where the symbol Σ in front of the integral denotes summation of the electron and hole contributions. The cyclotron mass m and the frequency Ω are positive for the electron sections of the Fermi surface and negative for the hole sections. The quantity $(mv_0)^2$ in (15) must be expressed with the aid of (11) in terms of the area of the cross section and the corrugation parameters.

It was already noted above that wave propagation near the DSCR of the holes take place if $\kappa \langle v_z \rangle \lesssim \Omega$. We can therefore neglect in (15) the spatial dispersion in the resonant denominators of all the terms except the first. We consider the case of low frequencies and

strong magnetic fields, when $\omega \ll \nu \ll \Omega$. Under these conditions, the nonlocal conductivity σ^+ , given by (15), can be transformed into

$$\sigma^{(+)}(\kappa) = \sigma_e^{(+)}(\kappa) + \sigma_h^{(+)}(\kappa) = i \frac{ec}{H} \left[\frac{N_e(\kappa)}{1+i\gamma_e} - \frac{N_h(\kappa)}{1-i\gamma_h} \right], \quad (16)$$

$$N_e(\kappa) = \frac{1}{4\pi^3} \int_{-k_e}^{k_e} dk_z S_e(k_z) \frac{1+i\gamma_e}{1+i\gamma_e + (\kappa/2\pi)u_e(k_z)}, \quad (17)$$

$$N_h(\kappa) = \frac{2}{4\pi^3} \int_{-k_B}^{k_B} dk_z \frac{S_h(k_z)}{1-W} \left\{ \frac{1-i\gamma_h}{1-i\gamma_h + (\kappa/2\pi)u_h(k_z)} - W \right\}, \quad (18)$$

where the subscripts e and h pertain to electrons and holes, $S_{\alpha}(k_z)$ is the area of the intersection of the corresponding part of the Fermi surface with the plane $k_z = \text{const}$ in k-space;

$$u_{\alpha}(k_z) = \frac{2\pi \langle v_{z\alpha} \rangle}{\Omega_{\alpha}} = -\frac{\hbar c}{eH} \frac{\partial S_{\alpha}}{\partial k_z} \quad (\alpha = e, h), \quad (19)$$

u_{α} is the displacement of the carriers during the cyclotron period,

$$W = \sum_{l=1}^{\infty} \left(\frac{\xi_l^2}{ls-1} - \frac{\eta_l^2}{ls+1} \right), \quad (20)$$

W is a parameter characterizing the corrugation of the Fermi surface, k_e is half the thickness of the electron lens along the k_z axis ($k_e = 0.28 \text{ \AA}^{-1}$ [17]), and $k_B = 0.57 \text{ \AA}^{-1}$ is half the height of the Brillouin zone. The first term in (16) describes the contribution of the electrons to the nonlocal conductivity, and the second the contribution of the holes. The expression (17) for $N_e(\kappa)$ does not contain the corrugation parameter W , since the electron lens has rotational symmetry and $\xi_l = \eta_l = \zeta_l = 0$ for it. In the derivation of (18) we have assumed that the hole monster is solid, and disregarded the hole pyramid inside the monster. In addition, we took into account the fact that the Brillouin zone contains two monsters (the factor 2 in the right hand side of (18)).

In the local limit, formulas (17) and (18) go over into the expressions for the electron and hole densities as $\kappa \rightarrow 0$. In cadmium they are equal, so that the following condition should be satisfied:

$$N_h(0) = N_e(0) = \frac{1}{4\pi^3} \int_{-k_e}^{k_e} S_e(k_z) dk_z = N_0. \quad (21)$$

Formula (17), which describes the electronic conductivity, is valid for all values of the wave vector κ , whereas expression (18) is valid only in the region (13), where the wavelength exceeds the hole displacement. We confine ourselves to just this region. In the calculation of $N_{\alpha}(\kappa)$ we assume that γ_{α} do not depend on k_z , since the carrier collisions are taken into account only qualitatively. In addition, we neglect the dependence of W on k_z , since $W(k_z)$ cannot have any singularities.

2. Nonlocal conductivity of the lens electrons. To find the explicit form of the functions $N_{\alpha}(\kappa)$, it is necessary to know the dependence of the intersection area S_{α} on k_z . To this end, we use plots of $\partial S_{\alpha} / \partial k_z$ based on the experimental data of Jones, Goodrich, and Falicov [17] and shown in Fig. 6. We consider first curve 1, which characterizes the change of the area of the lens section. As seen from the figure, $\partial S_e / \partial k_z$

increases linearly at small k_z and flattens out as $k_z \rightarrow k_e = 0.28 \text{ \AA}^{-1}$. This curve can be approximated by a function in the form

$$\frac{\partial S_e}{\partial k_z} = -2\pi k_0 \left[1 - \left(1 - \frac{k_z}{k_e} \right)^n \right] \text{sign } k_z, \quad (22)$$

where k_0 is the curvature radius of the lens at the limiting point, and n is an exponent that can be varied. We assume $k_0 = 1.5 \text{ \AA}^{-1}$. The value of the function (22) at $k_z = k_e$ coincides here with the maximum value of $\partial S / \partial k_z$ for the curve of Fig. 6. The value of the radius of curvature is also in good agreement with the limiting value of the oscillation period of the electronic doppleron^[1].

Integrating (22), we obtain the dependence of the area S_e on k_z :

$$S_e(k_z) = 2\pi k_0 k_e \left[1 - \frac{|k_z|}{k_e} - \frac{1}{n+1} \left(1 - \frac{|k_z|}{k_e} \right)^{n+1} \right]. \quad (23)$$

Specification of the exponent n uniquely determines the shape of the lens. At $n = 1$, Eq. (23) describes an oblate ellipsoid of revolution, the section of which in the plane $k_x = 0$ is represented by curve 1 of Fig. 7. Curve 2 and 3 of Fig. 7 correspond to $n = 2$ and $n = 3$. The same figure shows the experimental points from Fig. 7 of [17]. We see that these points fit best the contour 2. The corresponding value of the radius of the lens in the plane $k_z = 0$ is $k_\perp = 0.75 \text{ \AA}^{-1}$. This agrees with the radius of the lens on Fig. 7 of [17], but differs from the value $k_\perp = 0.78 \text{ \AA}^{-1}$ given in Table III of the same paper. The value $k_\perp = 0.78 \text{ \AA}^{-1}$ corresponds better to the case $n = 3$. An ellipsoid of revolution ($n = 1$) gives too small a lens radius and agrees poorly with the experimental points. We note that the area of the contour 2, namely 0.613 \AA^{-2} , is in good agreement with the value $S_e(0) = 0.608 \text{ \AA}^{-2}$ obtained by Grassie from measurements of the de Haas-van Alphen effect. Finally, at $n = 2$ the function (22) coincides almost exactly with curve 2 of Fig. 6, which is based on the data of [17].

Figure 7 shows also a dashed contour, which represents the lens produced by combining two spherical segments with radius $k_0 = 1.5 \text{ \AA}^{-1}$. In our earlier paper^[1] we used the spherical-lens model to describe the properties of the electronic doppleron. The radius of curvature was assumed equal to the Fermi wave vector $k_0 = 1.42 \text{ \AA}^{-1}$ of the free-electron sphere. This value of k_0 yields too low a value of the period of the doppleron oscillations. We shall discuss later on the results obtained with the model of a spherical lens with radius $k_0 = 1.5 \text{ \AA}^{-1}$.

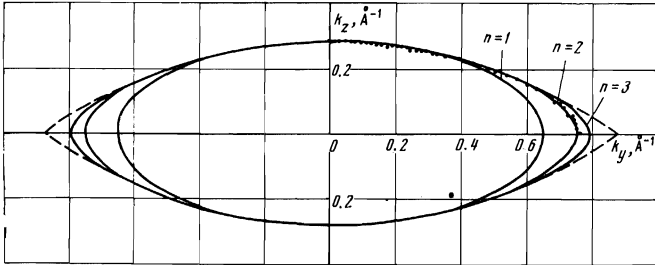


FIG. 7. Shape of the section of the lens in the $A\Gamma K$ plane for different models at $k_e = 0.28 \text{ \AA}^{-1}$ and $k_0 = 1.5 \text{ \AA}^{-1}$. The dashed curve corresponds to a lens made up of two spherical segments. The experimental points from [17] agree best with the case $n = 2$.

We now substitute (19), (22) and (23) in (17), introduce a new integration variable $x = 1 - |k_z|/k_e$ in place of k_z , and transform the expression for N_e into

$$N_e^{(n)}(q) = \frac{k_0 k_e^2}{2\pi^2} \int_0^1 \left[\frac{1}{1+q(1-x^n)} + \frac{1}{1-q(1-x^n)} \right] \left(1 - \frac{x^n}{n+1} \right) x dx, \quad (24)$$

$$q = \frac{\kappa u_0}{2\pi} \frac{1}{1+i\gamma_e}, \quad u_0 = \frac{2\pi\hbar k_0 c}{eH}, \quad (25)$$

where u_0 is the displacement of the limiting-point electrons during the cyclotron period. In the long-wave region, where $|q| \ll 1$, we have

$$N_e^{(n)} = N_0^{(n)} \left[1 + q^2 \frac{n^2(3n+5)}{(n+1)(n+3)(3n+2)} \right], \quad (26)$$

$$N_0^{(n)} = \frac{k_0 k_e^2}{2\pi^2} \frac{n(n+3)}{(n+1)(n+2)}. \quad (27)$$

At the values of k_0 and k_e chosen by us and at $n = 2$, the electron density is $N_0^{(2)} = 0.5 \times 10^{22} \text{ cm}^{-3}$. Calculation of the integral (24) for arbitrary values of q also entails no difficulty. For example, for $n = 2$ we obtain

$$N_e^{(2)}(q) = \frac{2N_0^{(2)}}{5q} \left[\ln \frac{1+q}{1-q} - \frac{1}{2q} \ln(1-q^2) \right]. \quad (28)$$

This expression is almost real in the region where the wavelength $2\pi/\kappa$ exceeds the maximum electron displacement u_0 . At shorter wavelengths, where $|\kappa u_0| > 2\pi$, the logarithms in (28) have finite imaginary parts describing the cyclotron absorption of the wave by the electrons.

3. Nonlocal hole conductivity. We proceed to calculate the function $N_h(\kappa)$ given by (18). The form of this function is determined by the character of variation of the area of the intersection of the monster with k_z . As seen from Fig. 6 (curve 2), the function $-\partial S_h / \partial k_z$ assumes a maximum value $S' = 2.5 \text{ \AA}^{-1}$ at $k_z = 0$ and decreases monotonically with increasing k_z , vanishing on the boundary of the Brillouin zone at $k_z = k_B$. As a rough approximation of curve 2 we can choose a line segment (shown dashed in Fig. 6) corresponding to the function

$$\frac{\partial S_h}{\partial k_z} = -S' \left(1 - \frac{|k_z|}{k_B} \right) \text{sign } k_z, \quad (29)$$

where $S' = 2.5 \text{ \AA}^{-1}$ and $k_B = 0.57 \text{ \AA}^{-1}$. Integrating (29), we obtain

$$S_h(k_z) = S_0 - S' (|k_z| - k_z^2 / 2k_B), \quad (30)$$

where $S_0 = S_h(0)$ is the area of the central section of the monster. The constant S_0 should be found from the condition that double the volume of the monster is equal to the volume of the electron lens. Integrating (30) from $-k_B$ to k_B and equating to half the volume of the lens, we get

$$S_0 = \pi^3 N_0 / k_B + 1/3 k_B S'. \quad (31)$$

The change of the area S_h on going from the central section of the monster at $k_z = 0$ to the section $k_z = k_B$ at the boundary of the Brillouin zone is $S' k_B / 2$. The relative decrease of the area is characterized by the parameter

$$\beta = S' k_B / 2S_0. \quad (32)$$

(We note that the monster is open if $\beta < 1$.) For the values of S' and N_0 assumed by us, $\beta \approx 0.96$.

We now substitute (29), (30), and (32) in (18) and integrate with respect to k_z . As the result, the expression for N_h takes the form

$$N_h(q) = \frac{N_0}{1-W} \left\{ \left[-\frac{\eta^2}{q^2} + \frac{\eta}{2q} \left(\frac{1}{\beta} - 1 + \frac{\eta^2}{q^2} \right) \ln \frac{\eta+q}{\eta-q} \right] \cdot \left(\frac{1}{\beta} - \frac{2}{3} \right)^{-1} - W \right\}, \quad (33)$$

where

$$\eta = \frac{2\pi k_0}{S'} \frac{1 - i\gamma_h}{1 + i\gamma_e} \approx 3.77 \frac{1 - i\gamma_h}{1 + i\gamma_e} \quad (34)$$

and q is given by the first formula of (25). In the region of relatively large wavelengths, where $q \ll \eta$, we have

$$N_h(q) \approx N_0 \left[1 + \frac{q^2}{3(1-W)\eta^2} \frac{1 - 2\beta/5}{1 - 2\beta/3} \right]. \quad (35)$$

It is seen from formula (33) that the hole conductivity has a logarithmic singularity as $q \rightarrow \pm\eta$. This singularity describes the Doppler-shifted cyclotron resonance due to the hole orbits near the central section of the monster. In the region $q^2 < \eta^2$, the expression (33) is almost real, and its value tends logarithmically to infinity as $q^2 \rightarrow \eta^2$. In the region $q^2 > \eta^2$ there appears a finite imaginary part describing the cyclotron absorption by the holes. We shall henceforth be interested only in the region $q^2 \lesssim \eta^2$.

4. Dispersion equation and its solution. For a circularly-polarized wave, Maxwell's equations lead to the following dispersion equation:

$$\kappa^2 = 4\pi i \omega c^{-2} \sigma^+(\kappa). \quad (36)$$

Using expression (16) for the nonlocal conductivity σ^+ and formula (25) for q , we can rewrite (36) in the form

$$\alpha = \Phi_+(q), \quad (37)$$

$$\Phi_+(q) = \frac{n(n+3)}{(n+1)(n+2)} \frac{1}{q^2} \left[\frac{N_h(q)}{(1-i\gamma_h)N_0} - \frac{N_e(q)}{(1+i\gamma_e)N_0} \right], \quad (38)$$

$$\alpha = \frac{\pi e H^3}{2h^2 c k_0^3 k_e^2 \omega} = \frac{1}{f} \left(\frac{H}{90} \right)^3, \quad (39)$$

where $N_h(q)$ in $N_e(q)$ are determined by the expressions (24) and (33), the explicit form of $N_e(q)$ for $n = 2$ is given by formula (28)). The wave frequency f in (39) is in Herz, and the magnetic field H in Oersteds. The parameter α depends on the frequency and on the magnetic fields, and is equal to the ratio ω_L/ω , where $\omega_L \sim H^3$ is the limiting frequency of the helicon that would exist in cadmium in the absence of holes.

We are interested in solutions of the dispersion equation (37) with almost real values of the wave vector $q = q' + iq''$ ($q'' \ll q'$), describing weakly damped waves. Such solutions can exist only in the case of strong magnetic fields and large mean free paths, when $\gamma_e, \gamma_h \ll 1$. Even under these conditions, however, the function Φ can have a finite imaginary part connected with the collisionless cyclotron absorption that sets in when $q^2 > 1$. For an explicit solution of (37) it is necessary to separate the real and imaginary parts of the function Φ_+ . Such a separation is a simple matter in the case when the imaginary part of the function Φ_+ is small compared with its real part:

$$\Phi_+(q) = \Psi_+(q') + i \left[q'' \frac{\partial \Psi_+}{\partial q'} + \Gamma(q') \right]. \quad (40)$$

The function $\Psi_+(q')$ is obtained from (38) by putting $\gamma_h = \gamma_e = 0$ and replacing q by q' . In addition, the

functions under the logarithm sign in (28) should be replaced by their absolute values. The function (q') can be approximated by the following formula (for the case $n = 2$)

$$\Gamma(q') = \frac{5}{6q'^2} \left[\gamma_e + \gamma_h + \frac{2\pi}{5|q'|} \left(1 + \frac{1}{2|q'|} \theta(|q'|-1) \right) \right], \quad (41)$$

where $\theta(x) = 0$ at $x < 0$ and $\theta(x) = 1$ at $x > 0$. The first two terms in the square brackets describe the wave damping due to carrier scattering; they are important in the region $|q'| < 1$, where the last term of (41) is equal to zero. The small terms γ_e and γ_h can be neglected in the region $|q'| > 1$ in comparison with the last term, which describes the cyclotron absorption by the lens electrons. The foregoing separation of the function Φ_+ into real and imaginary parts (40) is not valid near the singular points ($q' = 0, |q'| = 1, |q'| = |\eta|$) at which the derivative $\partial \Psi_+ / \partial q'$ vanishes or becomes infinite. Far from these points, the spectrum and the damping of the wave are determined by the equations

$$\alpha = \Psi_+(q'), \quad (42)$$

$$q'' = -\Gamma(q') \sqrt{\frac{\partial \Psi_+}{\partial q'}}. \quad (43)$$

Equation (42), with allowance for (39), can be rewritten in the form

$$H = G_+(q'), \quad (44)$$

$$G_+(q) = 90 [f \Psi_+(q')]^{1/3}, \quad (45)$$

in which a graphic solution is convenient. The form of the function Ψ_+ , and consequently of G_+ , depends on the number n which determines the shape of the lens (cf. (23)). In addition, Ψ_+ and G_+ depend on the corrugation parameter W . This dependence is significant near the DSCR of the holes at $q' \approx \eta$ and is practically nonexistent in the vicinity of the DSCR of the electrons in the region $q' \approx 1$. We shall therefore first calculate $G_+(q')$ for different n in the absence of corrugation ($W = 0$), and then discuss the changes brought about by the corrugation.

Plots of $G_+(q')$ at $f = 10^6$ Hz for $n = 1, 2, 3$ and for a spherical lens are shown in Fig. 8. We consider first curve 2, which corresponds to the case $n = 2$. At $|q'| \ll 1$, the function G_+ is determined by formulas (45) and (38) and by the asymptotic expansions (26) and (35). This limiting value is equal to -5.8 kOe. With increasing $|q'|$, the absolute value of G_+ increases, and as $|q'| \rightarrow 1$ it goes to $-\infty$ logarithmically. The fact that Φ_+ and G_+ are negative in the interval $|q| < 1$ means that the dielectric constant is negative for a wave whose field rotates in the same direction as the holes, and positive for a wave with opposite direction of field rotation. Thus, at the frequency $f = 1$ MHz in magnetic fields $H > 5.8$ kOe, the dispersion equation (44) has a real solution, i.e., the wave due to DSCR of electrons (electronic doppleron) can propagate in cadmium. At $H < 5.8$ kOe, the propagation of an electronic doppleron is impossible.

Variation of the shape of the lens leads to a change in the spectrum of the electronic doppleron. First, the lower field limit changes. Thus, for $n = 1$ (curve 1 on Fig. 8) the lower limit is 4.3 kOe and for $n = 3$ (curve 3 on Fig. 8) $H_{\min}^e = 6.6$ kOe. The experimentally observed limit is at $H = 6.2$ kOe, which agrees best with

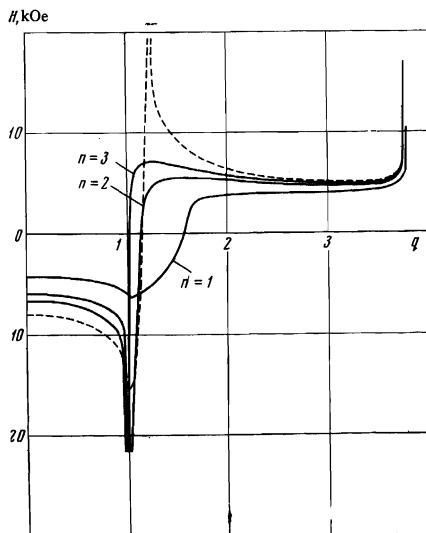


FIG. 8. Plots of the function $G_+(q')$. The dashed curve corresponds to the spherical lens.

the case $n = 2$ (the observed value of H_{\min}^e should be somewhat larger than the theoretical one). In addition, the shape of the lens influences the spectrum of the doppleron in strong fields. Thus, at $n = 1$ there is an end point (upper limit) of the spectrum at $H = 6.2$ kOe. For $n = 2$ and $n = 3$, there is no end point of the spectrum, since Ψ_+ and G_+ become infinite as $q' \rightarrow 1$. In the experiments, the oscillations are observed up to fields $H \sim 15$ kOe, the maximum of the amplitude is reached in the region of 10 kOe. Thus, the case $n = 1$ does not agree with the experimental data, and the cases $n = 2$ and $n = 3$ do not contradict the experiment. However, the behavior of the oscillations in strong fields does not permit a choice between these two cases. It is likewise impossible to ascertain whether an upper limit of the electronic doppleron exists, since the small-oscillation amplitudes observed in fields $H > 15$ kOe can be connected either with the doppleron or with the Gantmakher-Kaner size effect.

In our earlier paper^[1] we used a free-electron model in which the lens consisted of two spherical segments with a curvature radius 1.42 \AA^{-1} and height 0.28 \AA^{-1} . This model gives a lower limiting field $H_{\min}^e = 7.5$ kOe and a spectrum end point $H_{\max}^e = 13.6$ kOe, and agrees better with experiment than an ellipsoid of revolution ($n = 1$). It overestimates, however, the lower limits, underestimates the upper limit, and underestimates somewhat the limiting value of the period of the doppleron oscillations. In addition, this model has a major shortcoming in that the edge of the lens is sharp. This circumstance affects strongly the behavior of the dispersion function $\Phi(q')$ in the region $|q'| > 1$. The presence of a sharp edge leads to two consequences. First, the collisionless cyclotron absorption of the wave by the electrons, which appears at $|q'| > 1$, exists only in a relatively narrow wavelength interval. In fact, for a lens with a sharp edge, all the electrons have displacements in the interval from u_0 to $0.8u_0$. The cyclotron absorption therefore exists only in the interval $1 < |q'| < 1.25$. At $|q'| = 1.25$, the cyclotron absorption vanishes jumpwise. This is the second consequence. In accordance with the

Kramers-Kronig relations, the real part of Φ at the point $q' = 1.25$ has an infinite discontinuity (the dashed curve of Fig. 8 shows the corresponding function G). In the region $|q'| > 1.25$ the function G_+ is positive, meaning that a wave with positive circular polarization can propagate. When q' changes from 1.25 to 3.2, the function G_+ drops from plus infinity to a value $G_{\min} = 5$ kOe, and then again increases and becomes infinite as $|q'| \rightarrow |\eta| = 3.77$. Thus, two solutions describing the propagating waves exist in magnetic fields $H > G_{\min} = 5$ kOe. The first, given by the left point of intersection of the dashed curve with the horizontal straight line $G_+ = \text{const} > G_{\min}$, describes a wave that can be called a "hole helicon." The second solution, given by the right-hand intersection point, describes a hole doppleron.

The situation is different if the lens has a rounded edge. In this case there are electrons with arbitrary displacements smaller than u_0 , which lead to the existence of cyclotron absorption at any $|q'| > 1$. Accordingly, the function G_+ does not have an infinite discontinuity, but varies smoothly (curves 1–3 in Fig. 8). The smoothest edge is possessed by the ellipsoid, and accordingly the function G_+ has the smallest dispersion at $n = 1$. In this case there is no solution describing a hole helicon at all, and the hole doppleron does not have a clearly pronounced lower magnetic-field limit. In the cases $n = 2$ and $n = 3$ there are solutions of the hole-helicon type, and this leads to the presence of a lower limit for the hole doppleron.

As seen from (43), the wave damping is greater the smaller the slope of the dispersion curve. Therefore the hole helicon has a much larger damping than the hole doppleron in the region $q' \rightarrow |\eta|$. The dependence of the damping length of the hole helicon and of the hole doppleron on the magnetic field is shown in Fig. 9. The curves were plotted for the case $n = 2$ and $f = 1$ MHz. We see that the damping length of the helicon does not exceed 0.02 mm, whereas the damping length of the doppleron increases rapidly with increasing field, approaching the mean free path of the holes, which was assumed equal to 0.4 mm. No oscillations that could be interpreted as helicons were observed in our experiments, but the hole doppleron had a clearly pronounced lower limit $H_{\min}^h = 4.7$ kOe. Thus, the Fermi-surface model considered by us gives good agreement with experiment. Allowance for the corrugation of the monster can modify somewhat the function G_+ and the

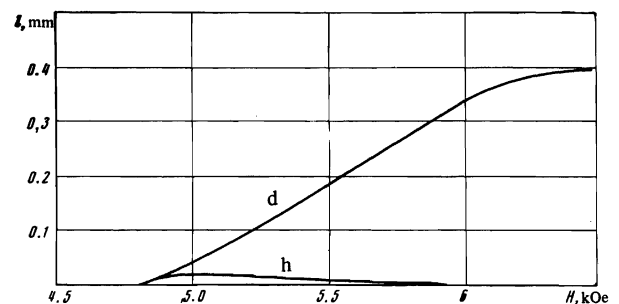


FIG. 9. Damping lengths of hole helicon (curve h) and of hole doppleron (curve d) vs the magnetic field for the case $n = 2$ and $W = 0$.

vicinity of the DSCR of the holes (at $q \leq \eta$) and shift the lower limit H_{\min}^h of the hole doppleron. It is seen from expression (20) for W that this value can be either positive or negative. In the case $W > 0$, the function $N_h(q)$, defined by formula (33), increases, as the result of which G_+ and the lower limit H_{\min}^h shift upward. At $W < 0$, to the contrary, the function G_+ and the limit H_{\min}^h decrease. The larger $|W|$, the more appreciable these changes. Since expression (20) contains both positive and negative terms, it is possible that $|W|$ is small and the corrugation of the monster exerts a weak influence on the properties of the hole doppleron.

The amplitude of the hole doppleron turns out to be much smaller than the amplitude of the electronic doppleron. Therefore the impedance oscillations due to the hole doppleron are observed only in the interval from H_{\min}^h to H_{\min}^e . Calculation shows that in the case $n = 2$ the change of the period of the oscillations of the hole doppleron in the field interval from 5.1 to 6 kOe is about 30%. This estimate agrees with the experimental data (see Fig. 3). It should be noted that near H_{\min}^e the slope of the dispersion curve of the hole doppleron is still not too large. Therefore the period of the doppleron oscillations in the region $H < H_{\min}^e$ should be smaller than the period of the Gantmakher-Kaner oscillations. This also agrees with experiment: the value of the derivative (2), obtained under the assumption that the limiting period is observed, is smaller than the value $S' = 2.5 \text{ \AA}^{-1}$ assumed by us. One final remark. When the magnetic field is inclined, the observed lower limit of the electronic doppleron shifts towards strong fields and the oscillations of the hole doppleron can be seen up to the new limit H_{\min}^e . This fact also indicates that there is no upper limit for the hole doppleron.

In conclusion, the authors thank V. G. Fastovskii for interest in the work, E. S. Itskevich for supplying the samples of pure cadmium, and A. V. Gavrilov and L. I. Radel' for technical help.

¹L. M. Fisher, V. V. Lavrova, V. A. Yudin, O. V. Konstantinov, and V. G. Skobov, *Zh. Eksp. Teor. Fiz.* **60**, 759 (1971) [*Sov. Phys.-JETP* **33**, 410 (1971)].

²D. S. Falk, B. Gerson, and J. F. Carolan, *Phys. Rev. B1*, 407 (1970).

³R. G. Chambers and V. G. Skobov, *J. Phys.* **1**, 202 (1971).

⁴O. V. Konstantinov and V. G. Skobov, *Fiz. Tverd. Tela* **12**, 2768 (1970) [*Sov. Phys.-Solid State* **12**, 2237 (1971)].

⁵V. A. Yudin and L. M. Fisher, **3**, 131 (1971).

⁶V. A. Yudin and L. M. Fisher, *ibid.* **2**, 1972 (in press).

⁷V. A. Yudin, *ibid.* **6**, 188 (1967).

⁸V. F. Gantmakher and É. A. Kaner, *Zh. Eksp. Teor. Fiz.* **48**, 1572 (1965) [*Sov. Phys.-JETP* **21**, 1053 (1965)].

⁹A. D. C. Grassie, *Phil. Mag.* **9**, 847 (1964).

¹⁰D. C. Tsue and R. W. Stark, *Phys. Rev. Lett.* **16**, 19 (1966).

¹¹J. K. Galt, F. R. Merrit, and J. N. Klauder, *Phys. Rev.* **139**, A823 (1965).

¹²M. P. Shaw, T. G. Eck, and D. A. Zych, *ibid.* **142**, 407 (1966).

¹³D. F. Gibbons and L. M. Falicov, *Phil. Mag.* **8**, 177 (1964).

¹⁴M. R. Daniel and L. Maccinnon, *ibid.* **8**, 537 (1963).

¹⁵V. P. Naberezhnykh, A. A. Mar'yakhin, and V. L. Mel'nik, *Zh. Eksp. Teor. Fiz.* **52**, 617 (1967) [*Sov. Phys. Phys.-JETP* **25**, 403 (1967)].

¹⁶R. G. Goodrich and R. C. Jones, *Phys. Rev.* **156**, 745 (1967).

¹⁷R. C. Jones, R. G. Goodrich, and L. M. Falicov, *ibid.* **174**, 672 (1968).

¹⁸R. W. Stark and L. M. Falicov, *ibid.* **19**, 795 (1967).

¹⁹É. A. Kaner and V. G. Skobov, *Adv. in Phys.* **17**, 605 (1968).

Translated by J. G. Adashko